LWIR Hyperspectral and Multispectral Scene Simulation of Mars

Steven Richtsmeier
Spectral Sciences, Inc., 4 Fourth Ave., Burlington, MA 01803
Robert Sundberg
Spectral Sciences, Inc., 4 Fourth Ave., Burlington, MA 01803
Raymond Haren
AFRL/SNJT, 3109 "P" Street Bldg 20622, Wright-Patterson AFB, OH 45433
Frank O. Clark
AFRL/VSBT, 29 Randolph Road, Hanscom AFB, MA 01731

ABSTRACT

Full optical spectrum (UV to LWIR) hyperspectral scene simulation provides an accurate, robust, and efficient means for algorithm validation and sensor design trade studies. This paper reviews the development of a first-principles, high-fidelity HSI/MSI image simulation capability, dubbed MCScene, which is based on Direct Simulation Monte Carlo techniques and demonstrates how the model can be used for sensor design trade studies. Basic features of the model will be discussed and illustrated with a spectral simulation for a prototype hyperspectral sensor. Sample calculations presented in this paper include long wave infrared spectrum simulations for a region of Mars under varying solar illuminations and atmospheric conditions. Source information for simulations will be based on mission data where available. Such simulations can be important for gauging the effects of the Martian atmosphere on mineral determination by orbiting multispectral imagers, for example.

1. INTRODUCTION

Remote hyperspectral and multispectral imagery (HSI and MSI) of the Earth has proven to be highly valuable for numerous applications, including mineral prospecting, environmental and land use monitoring, and military surveillance and reconnaissance. The quality of the data products depends critically on the accuracy of the atmospheric compensation, surface reflectance or emissivity/temperature retrieval, detection/identification and other algorithms. Thus, there is a need for accurate, robust, and efficient means for algorithm validation. For this purpose, simulated imagery can provide a practical alternative to field measurements, which are typically expensive, time consuming, and impractical for covering the full range of anticipated atmospheric and surface conditions. The utility of simulated imagery is not necessarily limited to terrestrial applications. Aerosols in the atmosphere of Mars, for example, have been found to influence the apparent spectra of Martian surface materials. Given fundamental characteristics of the Martian atmosphere and its aerosols, simulations could be used to determine atmospheric effects on the apparent spectra of any material for a broad spectrum of atmospheric conditions and observation and illumination scenarios.

1.1 High-fidelity Model Description

The MCScene code originated from a Phase II SBIR program with NASA Stennis for development of "A 3D Radiative-Transfer Hyperspectral Image Simulator for Algorithm Validation [1]." Its features include:

- 3D simulation of radiative transport (RT) effects spanning wavelengths from the UV through the SWIR,
- full treatment of molecular absorption and Rayleigh scattering, aerosol absorption and scattering, and multiple scattering and adjacency effects,
- calculation of reflections from a topographic terrain or from faceted 3D objects embedded in the scene, and
- scattering by, and transmission through, clouds.

The representation of the computational region is laid out in Fig. 1 (left). The calculation surface footprint is a 50 km x 50 km square. The sensor field-of-view (FOV) is at the center of this region. For data management reasons, 10^8 pixels represents a practical upper limit to the number of pixels in a scene. This allows us to represent, for example, an FOV region of 10 km x 10 km square gridded with 1 m^2 pixels. The area outside the sensor FOV is assigned uniform surface material properties to model adjacency effects, i.e., to account for photons that strike the ground outside the sensor FOV, undergo multiple scattering events, and scatter into the FOV. The atmosphere above 15 km is represented by homogeneous 100 m layers. Below 15 km, the atmosphere is represented by voxels 100 m on a side.

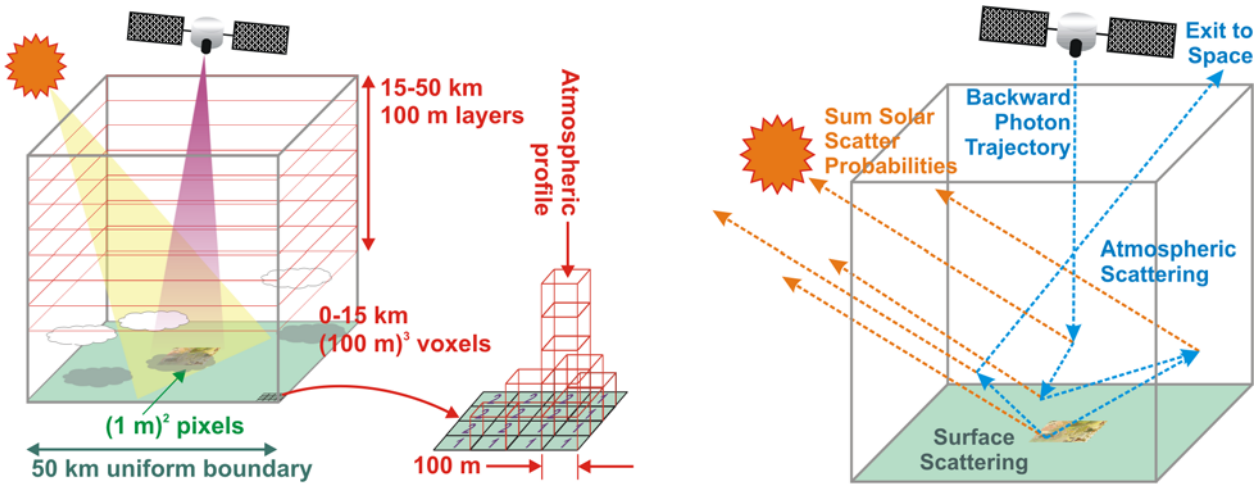

Fig. 1. Elements of the scene definition in the simulation model (left), and illustration of the backward DSMC approach used by MCScene to track trial photons (right).

A backward Monte Carlo (MC) radiative transport approach is employed (see the right of Fig. 1). It generates detailed, realistic, and accurate hyperspectral radiance images of spatially varying surfaces observed through a 3D atmosphere. The model is explicitly tied to MODTRAN5 spectroscopy [2] for the gaseous species and optical properties for clouds and aerosols. The major advantages of the MC methodology over other scattered radiance techniques are its simplicity, accuracy, and versatility, enabling rigorous modeling of complex 3D scenes.

1.2 Sample Simulations

The capabilities of MCScene are illustrated in Fig. 2. The scene at left was constructed from an AVIRIS reflectance cube of the Virgin Mts., NV that was atmosphere-compensated with FLAASH [3,4] and de-shadowed using an iterative matched filter technique [5]. (It is necessary to remove the natural shadows from the original image so that they don't conflict with those generated by MCScene.) The reflectance map was laid over a USGS 10 m digital elevation map for this region to provide terrain information. MODTRAN's mid-latitude summer atmosphere and desert aerosol models were utilized for the simulation atmosphere. A nadir-viewing sensor at 20 km altitude looks down on a synthetic nimbostratus cloud field generated by the Cloud Scene Simulation Model [6] and inserted into the scene with its base at 150 m above the underlying terrain. The sun is placed in the southwest with a zenith angle of 44°.

In the right of Fig. 2, a simple facet model of an oversized house has been embedded into a scene based on an atmosphere-compensated AVIRIS cube of the NASA Stennis Space Center. The house has pine wood walls, red asphalt shingles, and a chimney of red smooth-faced brick. Material properties were taken from the Johns Hopkins University "mammade2" materials library packaged with the ENVI software package [7]. The simulation atmosphere was MODTRAN's mid-latitude summer with rural aerosols and 20 km visibility. The sensor is at 2 km altitude and a zenith angle of 60°. The solar zenith angle is 44°. Close examination of the house shows that it casts a shadow on the ground, and the chimney at the front of the house casts a shadow on the roof and front wall. MCScene 3D objects are an integral part of the simulation, interacting with their surroundings. They cast shadows on the ground, are shadowed by 3D terrain or clouds, and their spectral signatures are affected by the intervening atmosphere in the same way as their surroundings. They are not stitched-in imagery.

Fig. 2. RGB MCScene simulations for (left) a synthetic nimbostratus cloud field over the Virgin Mts., NV, and (right) a facet model of an oversized house embedded in a scene at the NASA Stennis Space Center.

2. MCSCENE SPEEDUP

Monte Carlo calculations are, in general, inherently computationally intensive, and MCScene is no exception to this rule. The power of the DSMC technique to handle large complex problems at a fine level of detail is coupled to its major drawback. It can be extremely computationally intensive and require, in the case of a full hypercube simulation, tens to hundreds of hours of computational time on a typical personal computer to achieve statistical convergence. These times are decreasing as computers become increasingly fast, but a more substantial decrease in execution time would make MCScene a much more powerful study tool.

The general rule of thumb utilized to estimate MCScene simulation times for non-cloudy scenes is 10^{-4} sec per photon per pixel (a little more for blue photons, a little less for red photons) on a 3 GHz microprocessor. Run-times are reasonable for small scenes with a few spectral bands, and individual pixels are calculated in a fraction of a second. However, a large hyperspectral simulation could require weeks of processor time. For example, a full AVIRIS scene with 512 x 512 pixels and 224 spectral channels, simulated with 1000 Monte Carlo photons per pixel would require over two months of computational time to complete on a single processor. This simulation includes Rayleigh, aerosol, and surface scattering from a 3D terrain, in which photons scatter 6 to 7 times on average. Generation of a scene that also includes clouds would require ten times the computational time because of the high degree of scattering associated with clouds. Clearly, decreasing MCScene execution times would give us the ability to generate and evaluate complex scenarios in a more timely manner.

We have been pursuing two approaches for code acceleration:

- parallelization of MCScene through implementation of MPI (Message Passing Interface), and
- adaptation of remote imagery compression techniques to MCScene hypercube generation.

The program structure of MCScene [1,8,9] is highly amenable to parallelization as the calculation for each sensor pixel as well as for each band is completely independent of the calculation of any other pixel or band. We have implemented the Message Parsing Interface (MPI) [10,11,12,13] to distribute the calculation work load across a number of processors. The acceleration scales roughly as the number of processes utilized. We are currently running MCScene running 40+ processes on a dedicated cluster.

Our preliminary estimates of overall speedup are that we will decrease our typical computational times by a factor of about 400 using a combination of parallelization and software acceleration techniques. This will allow us to use MCScene to perform extensive parametric studies for scenarios in which the effects of changing atmospheric properties, sensor characteristics, viewing and illumination scenarios, and surface properties can be examined.

2.2 Software Acceleration Algorithm

2.2.1 Overview of the Sequential Maximum Angle Convex Cone (SMACC) Code

There is a substantial amount of spectral redundancy in a full hyperspectral image cube. Taking advantage of this redundancy could speed MCScene considerably. For example, consider a scene with a grass pixel having two hundred spectral channels. One could choose perhaps a dozen spectral channels from which one could classify as characteristic of "grass". The full spectra of other grass pixels in the scene could then be extrapolated based on examination of these twelve channels for "grassiness". To extend this idea, if we could classify all pixels in a scene in terms of a few "pure" materials based on a few spectral channels, we would be able to extrapolate the full spectra of all pixels based on the full spectra of the pure materials.

A very promising and novel classification technique is based on the SSI-developed Sequential Maximum Angle Convex Cone (SMACC) code [14,15]. This code was originally developed for analysis of remote sensing imagery. SMACC automatically and rapidly finds spectrally pure pixels, called end members, whose positive linear combinations fit the scene spectra to high accuracy. SMACC also simultaneously calculates the combination coefficients (abundances) and the fit residuals. SMACC provides an automated and rapid means to both find the end members and perform the unmixing. It is unique among end member codes in its automation and speed.

With SMACC, the HSI/MSI image is automatically decomposed into convex-cone end members, which include end-images and end-spectra. The former are the images for spectral channels that contain the most unique spatial information; the latter are spectra of pixels that represent the most unique spectra in the scene. The end members are selected in the order of significance to reconstruction. Simultaneously, abundance maps are calculated for each end member, providing the spatial context for each end-spectrum, and the spectral context for each end-image. The image can be uniquely and completely represented by a full set of end members.

Plotting the spectral abundances for the end images of representative radiance data will aid us in selection of the most important bands for representing end members. We will be using end member spectra and spatial abundances derived from analysis of MCScene multispectral simulations to produce full spectrum data cubes.

2.2.2 Application of Unmixing Techniques to MCScene Speed-up

We will apply SMACC to aid in the speed-up of hyperspectral MCScene simulations, specifically, in the time-consuming Monte Carlo part of the engine used to calculate multiple scattering effects. The improved calculation scheme is outlined as follows:

1. Select spectral channels from a SMACC spectral abundance analysis of representative radiance data.
2. Perform MCScene calculations for all pixels on a spectrally sparse grid.
3. Analyze the result with SMACC to determine end members for the multispectral scene of (1).
4. Fit the multispectral scene with the end members as a basis set to yield an end member abundance map.
5. Perform the full spectrum MCScene calculation for the end member pixels.
6. Construct a full spectrum scene from a linear combination of the end member pixel spectra and the end member abundance maps.

This algorithm effectively performs a hyperspectral simulation while requiring only the computational time of a multispectral simulation.

Figs. 3-5 illustrate the approach with an AVIRIS apparent reflectance cube of a White Mts. scene (Fig. 3 top left) containing predominately green vegetation, sunlit clouds, soil, a road, and shadows. A multispectral data cube was formed from ten of the 224 spectral channels and processed by SMACC to produce 100 end members and their spatial abundance maps. Fig. 3 (top right) shows spectra of four of these end members. The symbols in the plot show the multispectral channels utilized. Corresponding abundance maps of the four end members represented in the spectral plot are shown across the bottom of Fig. 3. The full 224 channel spectra of the 100 end members along with their abundance maps were used to reconstruct a full spectrum reflectance cube. Fig. 4 displays RGB composites from the original reflectance cube (left) and the reconstructed cube (right). Visually, the two images appear to be nearly identical. Fig. 5 compares original and reconstructed spectra for a few non-end member pixels, and shows that the original spectra are reproduced to within better than 1% by the reconstruction process. Overall, the potential

speedup to be realized for a case such as this is the ratio of the full number of spectral channels (224) to the number of multispectral channels utilized to determine the end members (10), or 22.4. Combining this with the factor of 18 speedup realized via MPI parallelization, the overall speedup is 400. This could of course be increased by adding more nodes to the cluster system.

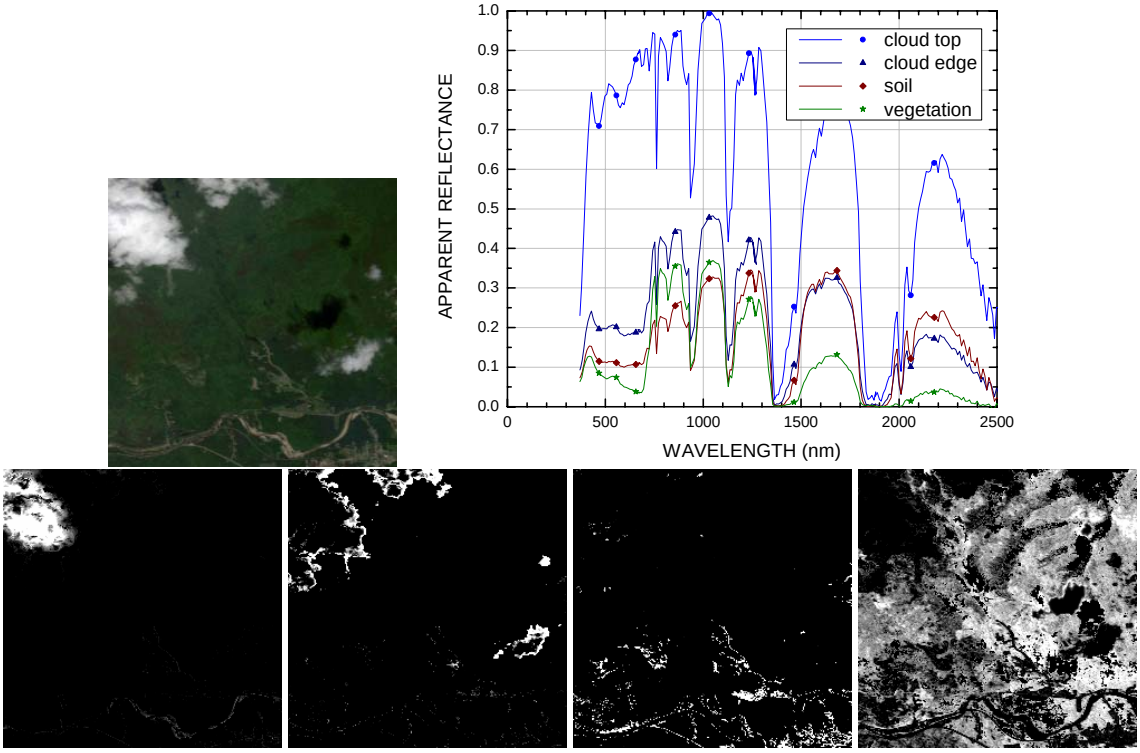

Fig. 3. Spectra of a few end members (top right) and their corresponding abundance maps (bottom) derived from the multispectral White Mts. reflectance data (top left). Symbols in the spectral curves correspond to the multispectral channels.

Fig. 4. Comparison of RGB composites of original (left) and reconstructed (right) White Mts. reflectance data.

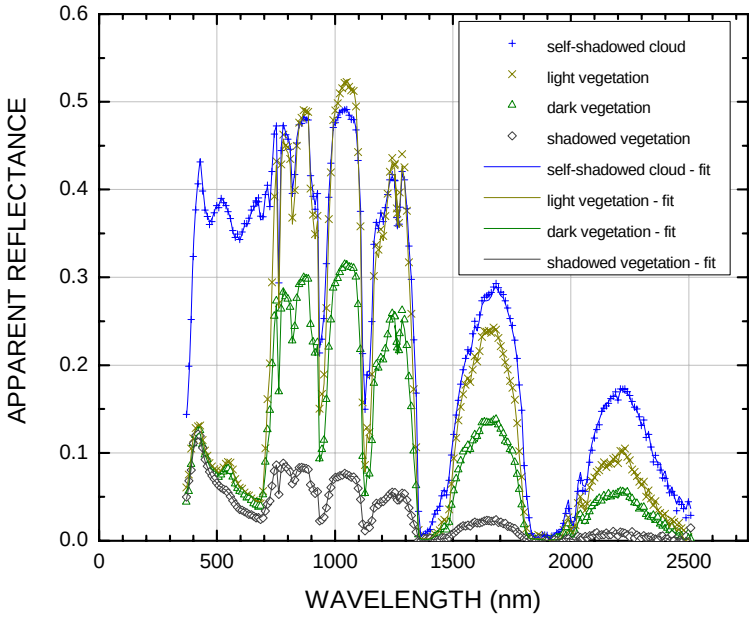

Fig. 5. Comparison of original and reconstructed spectra for a few non-end member pixels.

2.2.3 Evaluation of the Acceleration Algorithm

In the near future, we will be extensively evaluating the acceleration algorithm against full spectral MCScene calculations performed on the recently assembled cluster. There will be errors introduced into calculated radiance cubes by the fitting technique, and they are related directly to how well the end members determined by SMACC represent the full scene. Fitting a multispectral scene to one per cent error typically requires ten to tens of end members depending on the complexity of the scene. The rate-limiting step for the above sequence is step (1), where we calculate multiple scattering for perhaps hundreds of thousands of pixels in a range of spectral channels. The timesaving is the time for the multispectral calculation compared to the time it would require to calculate the radiance for all spectral channels. Issues to be investigated include:

- How many spectral channels do we need in for the multispectral calculations, and how do we choose them?
- How many end members are required to adequately fit the multispectral scene?
- How does the statistical noise inherent to Monte Carlo calculations affect the goodness of fit?
- How does scene complexity, i.e., clouds, inhomogeneous atmosphere, terrain, shadowing, affect performance?

3. EXTENSION TO MARTIAN SCENARIOS

MCScene was extended to simulation of Martian scenarios by assigning measured Martian properties to the simulation components. Fig. 6 illustrates the results of a simulation series in which a sensor at 50 km altitude looks down at the Martian surface while the sun is moved across the sky. A digital elevation map of the Tithonium Chasma region (5°S, 287°E), derived from Viking measurements [16], was used to represent the terrain. The DEM has a horizontal resolution of roughly 200 m. It is characterized by a series of circular depressions and by valleys running roughly E-W. The terrain was painted with a uniform reflectance of a light soil as measured by the Spirit Pancam imager in Gusev crater [17]. Temperature and density profiles were taken from Pathfinder measurements [18]. The atmospheric visibility was set to 150 km, ie., there are no appreciable aerosols in the scene. Since the surface is spectrally uniform, all variation in the scene is due to illumination effects. In the early morning, the sun lights up the western sides of depressed terrain, while the eastern sides are shadowed. As the sun moves across the sky, the shadows move around to the eastern sides of depressions.

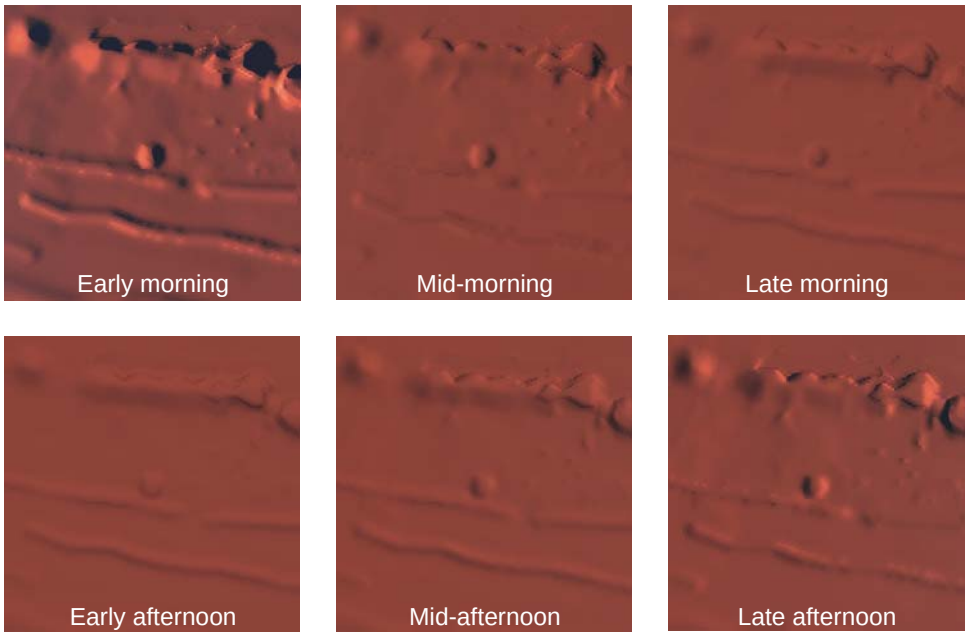

Fig. 6. Simulation sequence of varying solar position for a sensor at 50 km looking down at Martian terrain under clear sky conditions.

In Fig. 7, the sensor is moved down to 20 km altitude, still looking at the same terrain with a mid-afternoon sun, and varying degrees of aerosol coverage are introduced into the scene. Scattering and absorption properties for Martian aerosols were derived from Pathfinder measurements [19]. In the figure, surface features are increasingly obscured as the visibility is decreased from 150 km (clear sky) to 25, 10, and finally 5 km. At 5km visibility, surface features are barely discernable. Overall, the scene becomes slightly darker, but maintains a red color.

Fig. 8 shows the effect of aerosols on the reflectance spectra of several materials as viewed by a multispectral sensor at 20 km altitude at mid-afternoon. For these simulations, the surface was flat and spatially uniform. Four materials were investigated, including a black (albedo=0) absorbing surface, dark and light soils from Gusev crater, and a white (albedo=1) reflecting surface. All light seen over the black surface necessarily arises from atmospheric scattering alone. As visibility is decreased over the black surface, the apparent reflectance of the scene increases, with red wavelengths preferred over blue wavelengths. For the case of the dark Gusev soil, decreasing visibility results in enhanced reflectance in the red and slightly decreased reflectance in the blue, enhancing the apparent "redness" of the scene. For the light-colored Gusev soil, the apparent reflectance decreases slightly at most wavelengths, though the effect is small. The light Gusev soil and Martian dust may be comprised of similar materials. Finally, decreasing the visibility over the "white" surface, decreases the apparent reflectance at all wavelengths, with the effect being most pronounced at the blue wavelengths. Again, the overall effect is to make the scene appear more red in color.

Though surface features appeared obscured by 5 km visibility aerosols in Fig. 7, clearly, Fig. 8 shows that a significant number of photons striking the surface still reach the sensor. The apparent reflectance of the "white" surface is still brighter than the light Gusev soil, which in turn is brighter than the dark Gusev soil, which is lighter than the "black" surface. The photons reaching the sensor have undergone multiple scattering events, losing much of the spatial information they carried about the surface, but they still retain spectral information. The overall effect of Martian aerosols on the apparent spectra of surface materials is a complex combination of scattering and absorption by the aerosols, and is dependent on aerosol density as well as surface properties and viewing and illumination angles. Simulation tools such as MCScene can help to illuminate the complications introduced to Martian remote sensing applications by the Martian atmosphere.

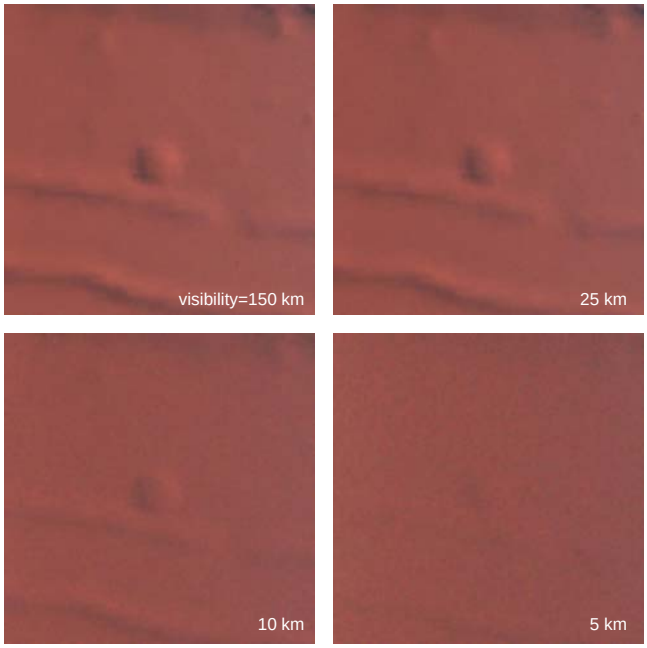

Fig. 7. Series of simulations illustrating the effect of decreasing visibility on the view of the Martian surface from a sensor at 20 km altitude with a mid-afternoon solar position.

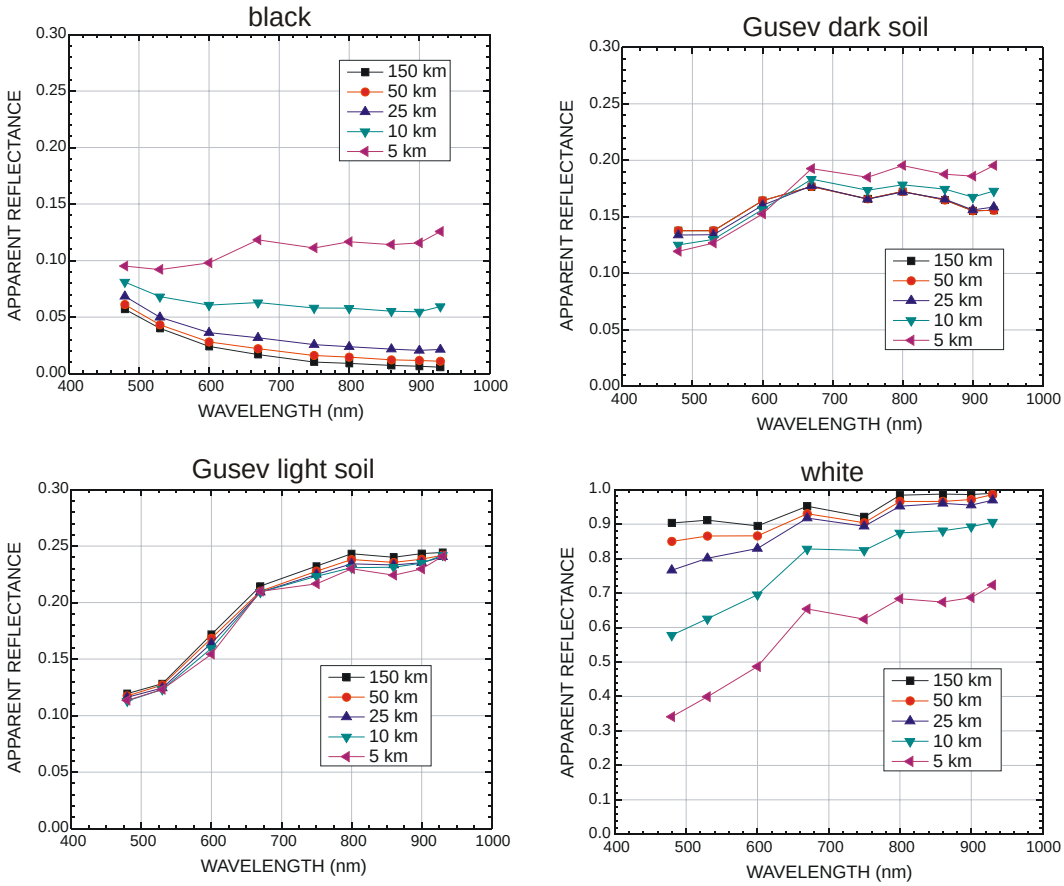

Fig. 8. Series of simulations illustrating the effect of decreasing visibility on apparent reflectance spectra of various materials from a sensor at 20 km altitude with a mid-afternoon solar position.

Fig. 9 shows results from another series of time-of-day simulations. A nadir-viewing sensor was placed at 20 km altitude over the Tithonium Chasma DEM. For these cases, the surface was painted with the spectral emissivity of Martian high albedo surface dust [20]. Surface temperatures were estimated from shadow maps and from pathfinder diurnal temperature variations (195-265 K). The images are false color composites plots with RGB corresponding to 500, 650, and 800 cm^{-1}, respectively. The figures have a magenta shading because radiation from the "green" band is mostly absorbed by atmospheric $_{CO2}$, and more light is emitted from the "red" band than from the "blue" band at these temperatures. Fig. 10 shows spectra of the center pixels for several of the simulations of Fig. 9. The dominant spectral feature is the CO_2 absorption band an 670 cm^{-1}.

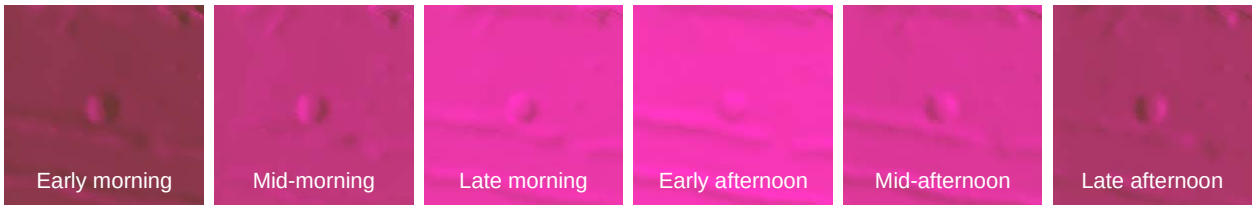

Fig. 9. RGB composites of LWIR simulations of Tithonium Chasma scenes.

Fig. 11 plots the atmospheric transmittance, and the upwelling and downwelling radiance for the center pixel of the late morning simulation of Fig. 9. The transmittance is near unity for all considered frequencies, except for the frequencies where the CO_2 absorption band becomes optically black. All radiance at the CO_2 band center in Fig. 10 comes from upwelling path radiance.

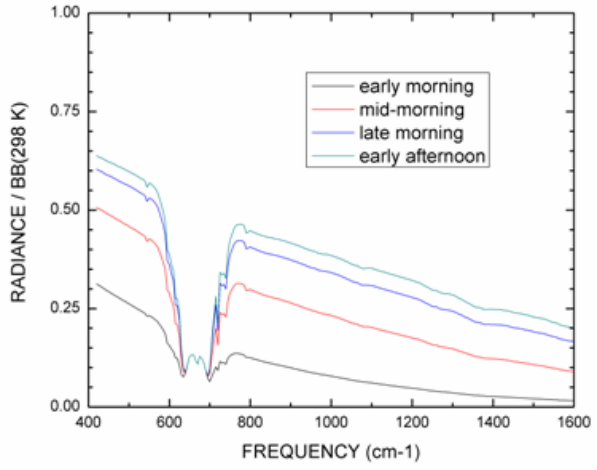

Fig. 10. Spectra of the center pixels for several of the simulations of Fig. 9.

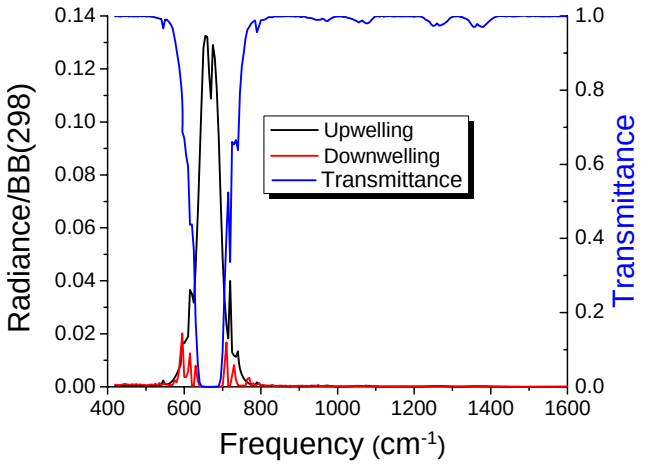

Fig. 11. Plots of transmittance and upwelling and downwelling radiance for the central pixel of the late morning case of Fig. 9.

4. SUMMARY

This paper has provided an overview of MCScene, a first principles, physics-based Monte Carlo hyperspectral scene simulation program. We have demonstrated a data driven simulation capability for full spectrum simulation of Martian scenes, including time-of-day variability, and the effects of aerosols and the atmosphere on the spectral properties of surface materials. Though the spatial resolution of these simulations was somewhat coarse, the fidelity of the simulations will improve as new information on Mars becomes available. MCScene simulations could provide a valuable tool for the evaluation of algorithms for identification of minerals on the Martian surface.

5. ACKNOWLEDGMENT

This work was supported in part by Air Force Research Laboratory/SNJT under Contract F33615-02-C-1167 and by Air Force Research Laboratory/VSBT under Contract HQ0006-05-C-7232.

6. REFERENCES

1. Richtsmeier, S., A. Berk, L.S. Bernstein, J.W. Duff and S.M. Adler-Golden, "A 3D Radiative-Transfer Hyperspectral Image Simulator for Algorithm Validation," Phase II Final Report, prepared for NASA Stennis Space Center under Contract No. NAS13-00025 (2002).
2. Berk, A., L. S. Bernstein, and D.C. Robertson, "MODTRAN: A Moderate Resolution Model for LOWTRAN 7," GL-TR-89-0122, Geophysics Directorate, Phillips Laboratory, Hanscom AFB, MA 01731 (April 1989) ADA214337
3. Adler-Golden, S.M., M.W. Matthew, L.S. Bernstein, R.Y. Levine, A. Berk, S.C. Richtsmeier, P.K. Acharya, G.P. Anderson, G. Felde, J. Gardner, M. Hoke, L.S. Jeong, B. Pukall, J. Mello, A. Ratkowski and H.-H. Burke, "Atmospheric Correction for Short-wave Spectral Imagery based on MODTRAN4," SPIE Proceeding, Imaging Spectrometry V, Vol. 3753 (1999).
4. Matthew, M.W., S.M. Adler-Golden, A. Berk, G. Felde, G.P. Anderson, D. Gorodetzky, S. Paswaters and M. Shippert, "Atmospheric Correction of Spectral Imagery: Evaluation of the FLAASH Algorithm with AVIRIS Data," SPIE Proc., Algorithms and Technologies for Multispectral, Hyperspectral, and Ultraspectral Imagery IX (2003).
5. Adler-Golden, S.M., M.W. Matthew, G.P. Anderson, G.W. Felde and J.A. Gardner, "An Algorithm for De-Shadowing Spectral Imagery," Presented at the AVIRIS Earth Sciences and Applications Workshop, at the NASA Jet Propulsion Laboratory (2002).
6. Cianciolo, M.E., and M.E. Raffensberger, "Atmospheric Scene Simulation Modeling and Visualization (AMV)," Cloud Scene Simulation Model User's Guide, TIM-07169-2, TASC, Reading, MA, (1996).
7. Research Systems, Inc., "ENVI, The Environment for Visualizing Images," Copyright (C) 2003, 4990 Pearl East Circle, Boulder, CO 80301, USA
8. Richtsmeier, S., A. Berk, S.M. Adler-Golden, and L.S. Bernstein, "A 3D Radiative-Transfer Hyperspectral Image Simulator for Algorithm Validation," Proceedings of ISSSR 2001, Quebec City, Canada (June 2001).
9. Sundberg, R.L., R. Kennett, S. Richtsmeier, J, Gruninger, A. Berk, and M. Matthew, "Hyperspectral Scene Simulation in the Ultraviolet through Longwave Infrared," SBIR Phase II Final Report, SSI-TR-453, (2005).
10. MPI Forum, *MPI: A Message-Passing Interface Standard*, Journal of Supercomputer Applications 8:157-416 (1994). Special issue on MPI.
11. MPI Forum, "MPI: A Message-Passing Interface Standard (version 1.1)," Technical report (1995). http://www.mpi-forum.org.
12. MPI Forum, "MPI-2: Extensions to the Message-Passing Interface," Technical report (1997). http://www.mpi-forum.org.
13. Gropp, W., E. Lusk, N. Doss, and A Skjellum, "A High Performance, Portable Implementation of the (MPI) Message Passing Interface Standard," Parallel Computing, 22, 789 (1996).
14. Gruninger, J.H., R. Sundberg, M. Fox, R. Levine, W. Mundkowsky, M.S. Salisbury, and A.H. Ratcliff, "Automated Optimal Channel Selection for Spectral Imaging Sensors," Proc. of SPIE, Orlando, FL, Vol. 4381, April (2001a)
15. Gruninger, J.H., M.J. Fox and R.L. Sundberg, "Hyperspectral Mixture Analysis using Constrained Projections onto Material Subspaces," Proc. of the International Symposium on Spectral Sensing Research, Quebec City, pp 162-170, June (2001b).
16. http://astrogeology/usgs.gov/Teams/photogrammetry/topography_mars.html
17. Bell, J.F. III et al., *Pancam Multispectral Imaging Results from the Spirit Rover at Gusev Crater*, Science, 305, 800 (2004).
18. Magalhães, J.A., J.T. Schofield, and A. Seiff, "Results of the Mars Pathfinder Atmospheric Structure Investigation," J. Geophys. Res., 104, 8943 (1999).
19. Markiewicz, W.J., R.M. Sablotny, H.U. Keller, N. Thomas, D. Titov, and P.H. Smith, "Optical Properties of the Martian Aerosols as derived from Imager for Mars pathfinder Midday Sky Brightness Data," J. Geophys. Res., 104, 9009 (1999).
20. Bandfield, J.L., T.D. Glotch, and P.R. Christensen, "Spectroscopic Identification of Carbonate Minerals in the Martian Dust," Science, 301, 1084 (2003).